Relative Strengths of Three Linearizations of Receptor Availability: Saturation, Inhibition, and Occupancy Plots

Javad Khodaii[1,2], Mostafa Araj-Khodaei[2], Manouchehr S. Vafaee[3–5], Dean F. Wong[6], and Albert Gjedde[3,5,7–9]

[1]*Department of Mechanical Engineering, Amirkabir University of Technology, Tehran, Iran;* [2]*Research Center for Integrative Medicine in Aging, Aging Research Institute, Tabriz University of Medical Sciences, Tabriz, Iran;* [3]*BRIDGE (Brain Research Inter-Disciplinary Guided Excellence), Department of Clinical Research, University of Southern Denmark, Odense, Denmark;* [4]*Research Unit for Psychiatry, Southern Region, University of Southern Denmark, Odense, Denmark;* [5]*Department of Nuclear Medicine, Odense University Hospital, Odense, Denmark;* [6]*Mallinckrodt Institute of Radiology, Washington University, St. Louis, Missouri;* [7]*Translational Neuropsychiatry Unit, Department of Clinical Medicine, Aarhus University, Aarhus, Denmark;* [8]*Panum Institute, Department of Neuroscience, University of Copenhagen, Copenhagen, Denmark; and* [9]*Neurosciences Research Center, Tabriz University of Medical Sciences, Tabriz, Iran*

We derived three widely used linearizations from the definition of receptor availability in molecular imaging with positron emission tomography (PET). The purpose of the present research was to determine the convergence of the results of the 3 methods in terms of 3 parameters—occupancy (s), distribution volume of the nondisplaceable reference binding compartment (V_{ND}), and nondisplaceable reference binding potential (BP_{ND}) of the radioligand—in the absence of a gold standard. We tested 104 cases culled from the literature and calculated the goodness of fit of the least-squares and Deming II methods of linear regression when applied to the determination of s, V_{ND}, and BP_{ND} using the goodness-of-fit parameters R^2, coefficient of variation (root-mean-square error [RMSE]), and the infinity norm ($||X||_\infty$) with both regression methods. We observed superior convergence among the values of s, V_{ND}, and BP_{ND} for the inhibition and occupancy plots. The inhibition plot emerged as the plot with a slightly higher degree of convergence (based on R^2, RMSE, and $||X||_\infty$ value). With two regression methods (the least-squares method [LSM] and the Deming II [DM] method), the estimated values of s, V_{ND}, and BP_{ND} generally converged. The inhibition and occupancy plots yielded the best fits to the data, according to the goodness-of-fit parameters, due primarily to absence of commingling of the dependent and independent variables tested with the saturation (original Lassen) plot. In the presence of noise, the inhibition and occupancy plots yielded higher convergences.

Key Words: PET; Lassen plots; inhibition plot; binding potential

J Nucl Med 2022; 63:294–301
DOI: 10.2967/jnumed.117.204453

PET is a major tool of biomedical research, with clinical applications that yield images of the distribution of systemically administered positron-emitting radionuclides in tomographic sections of the bodies of human subjects and experimental animals (*1*,*2*). Positrons are positively charged anti-electrons emitted from the nuclei of short-lived isotopes typically produced in a cyclotron. Users of this technique image the high-energy (511 keV) annihilation photons that result from the interaction of a positron with electrons in the tissue. PET images are reconstructed by means of computed tomography of the source of radioactivity, after injection of radiopharmaceuticals according to the principles of nuclear medicine (*3*). The imaging of neuroreceptors with radioactive ligands by PET applied to living mammalian brains makes it possible to determine receptor density and affinity by appropriate mathematic models (*4*).

Neuroreceptor studies of brain in vivo using PET require comparisons of so-called binding potentials of radiopharmaceutical receptor ligands at more or less inhibited receptor states to obtain estimates of receptor density and affinity (*5*). Naganawa et al. (*6*) proposed methods that reduce bias and variability, and the best use of these approaches is realized by improving the accuracy of data covariance matrices.

The quantitative determination of binding potentials uses a fundamental equation of receptor availability to obtain separate estimates of radioligand volumes of distribution of a specific radioligand (*5*,*7–10*). Application of any one of the three linearizations presented here is the first step toward determining binding potentials (or receptor availabilities), the foundation of the receptor-binding analysis. For situations in which a proper reference region with no specific binding of the ligand is not known to exist, or is known not to exist, three linearized versions of a receptor availability equation were derived to estimate the magnitude of the volume of distribution of nondisplaceable ligand (V_{ND}) by linear regression. The three different plots emerged when the equation of receptor availability was linearized differently by Lassen et al., Gjedde and Wong, and Cunningham et al. (*11–13*). Here, the three different plots are referred to as the Saturation, Inhibition, and Occupancy plots, to avoid the uncertain naming of the plots associated with the presentation of the Occupancy plot solution (*12*), referred to by some authors as the Lassen plot rather than the plot that Lassen et al. (*11*) actually used and reported. The Occupancy and Saturation plots commingle the dependent and independent variables by calculating the difference between the volume estimates for baseline and inhibition states, unlike the Inhibition plot, which simply plots the apparent total volume of distribution of the radioligand (V_T, also known as the partition volume or partition coefficient of the ligand) at inhibition ($V_{T(i)}$, ordinate) against the values at baseline ($V_{T(b)}$, abscissa).

The aim of the present research was to determine the accuracy and precision of these three widely used linearizations of receptor

Received Dec. 15, 2020; revision accepted Apr. 23, 2021.
For correspondence or reprints, contact Albert Gjedde (albert.gjedde@clin.au.dk).
Published online Jun. 4, 2021.

availability (Saturation, Inhibition, and Occupancy plots) from experimental data. We compared 104 cases culled from the literature, with the accuracy of each plot being evaluated by the least-squares and Deming II methods of linear regression.

MATERIALS AND METHODS

The quantitative determination of binding potentials uses a fundamental equation of receptor availability to obtain separate estimates of radioligand volumes of distributions for a specific radioligand (*5*,*7*–*10*):

$$1-s = \frac{V_{T(i)} - V_{ND}}{V_{T(b)} - V_{ND}} \quad (1)$$

where Equation 1 is the formulation of the relative or fractional receptor availability in terms of the relevant volumes of distribution. Here, s represents the occupancy and $V_{T(i)}$ is the apparent total volume of distribution of the sum of the specifically bound and the nonspecifically dissolved ligand molecules occupying the receptor, whereas V_{ND} refers to the distribution volume of the tracer in a nonbinding compartment, also known as the partition volume or partition coefficient of the ligand. $V_{T(b)}$ refers to the apparent total volume of distribution of the radioligand in a baseline state where the receptor is not occupied by a specific inhibitor.

Application of any one of the three linearizations presented here is the first step toward determining binding potentials (or receptor availabilities), the foundation of the receptor-binding analysis. The nondisplaceable reference binding potential (BP_{ND}) enters into the particular Eadie–Hofstee version of the linearized Michaelis–Menten equation that yields both the maximum binding (B_{max}) and the affinity constant (Michaelis half-saturation quantity or mass), K_D, of the receptors,

$$B = B_{max} - K_D \, BP_{ND} \quad (2)$$

where B is the quantity of bound ligand. The binding potential is defined as the ratio of the volumes of distribution of specifically bound (displaceable) and non-specifically bound (non-displaceable) ligand quantities (*14*,*15*). To determine the binding potential of a radioligand, the volumes of distribution are entered into the relationship that defines the binding potential (*2*,*5*,*16*):

$$BP_{ND} = \frac{V_T - V_{ND}}{V_{ND}} \quad (3)$$

which is applicable both to the receptor binding baseline and to multiple degrees of receptor blockade, provided the V_{ND} estimate is unaffected by the blockade. To calculate binding potentials, it is necessary to know the distribution of unbound ligand in a region of no binding, but a suitable reference region often does not exist or is not known to exist.

The three linearizations evaluated here served to determine a reference volume of distribution of radioligands when no reference region (i.e., a region with absence of specific binding) is known to exist in the brain. From the volumes of distribution of the radioligand in the absence of displaceable binding (V_{ND}), we used the three different linearizations to obtain binding potentials for radioligands used in published studies.

Saturation Plot

As a novel steady-state approach to determining the binding potentials of tracers with an unknown reference volume of distribution, in 1995, Lassen et al. (*11*) proposed to compare two levels of receptor occupancy, one essentially at zero for the labeled tracer itself and the other in the midrange of occupancy by addition of unlabeled ligand. The concentration of the unlabeled ligand in brain water would be zero in the tracer-alone study and would have a constant value in the inhibition studies. To obtain the volume of nonspecific binding, Lassen et al. (*11*) linearized Equation 1 in the form of the plot we here call the Saturation plot. The plot yields the estimate of V_{ND} by plotting the baseline volume of distribution ($V_{T(b)}$) as a function of the difference between the baseline and inhibition volumes of distribution ($\Delta V_T = V_{T(b)} - V_{T(i)}$) as shown in Figure 1A,

$$V_{T(b)} = \frac{1}{s}\Delta V_T + V_{ND} \quad (4)$$

where the estimate of V_{ND} is the ordinate intercept of the linear regression, and the estimate of the ratio $1/s$ is the slope of the regression.

Inhibition Plot

Certain receptor ligands tend altogether to lack a reference brain region of no specific binding, from which it is therefore not possible to assess nonspecific binding for the purpose of calculating the binding potential in regions of specific binding. Realizing that the uncertain choice of a reference volume of distribution for the ligand can lead to an erroneous estimation of the occupancy, in 2000, Gjedde and Wong (*12*) proposed to linearize Equation 1 to obtain the form of the

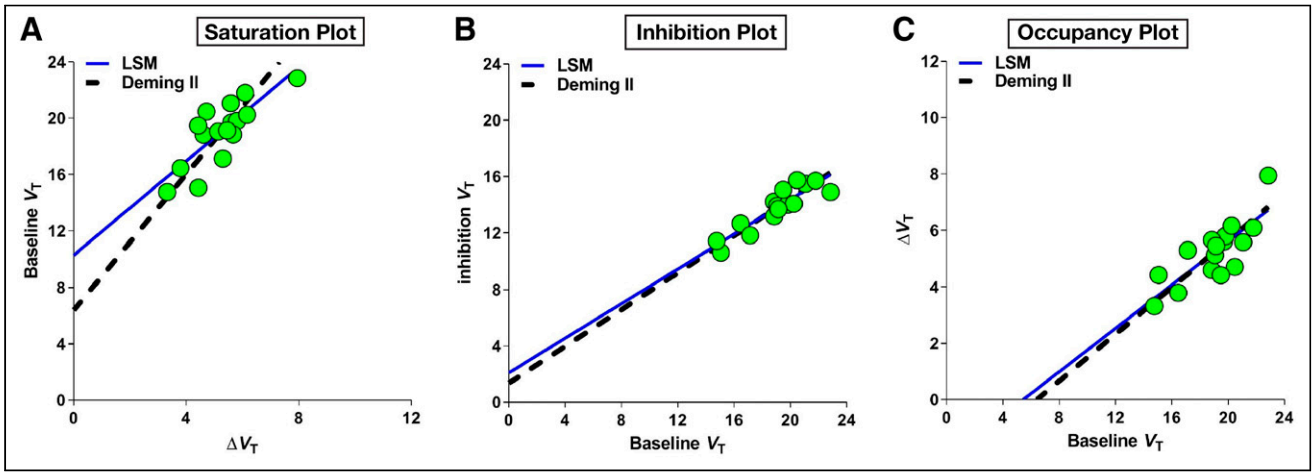

FIGURE 1. Three linearization plots ([A] Saturation, [B] Inhibition, [C] Occupancy) of data from Horti et al. (*17*) (inhibition dose 0.5 mg).

Inhibition plot. The plot estimates V_{ND} by relating $V_{T(i)}$ to $V_{T(b)}$ by linear regression, as shown in Figure 1B,

$$V_{T(i)} = (1-s)V_{T(b)} + s\ V_{ND} \quad (5)$$

where the estimate of V_{ND} is the intercept of the linear regression line with the line of identity.

Occupancy Plot

In 2010, Cunningham et al. (*13*) inverted the axes of the Saturation plot and showed that the graphical analysis of the inverted relationship at each of the different doses of unlabeled ligand provided a means to determine drug occupancies. The inversion of the axes of the Saturation plot was presented as the *Occupancy plot,* a term we adopt here to avoid the lack of specificity of the term *Lassen plot.* The linearization known as the Occupancy plot treats the differences in the volumes of distribution between the baseline and challenge conditions, ΔV_T, as a function of the baseline volume of distribution, as shown in Figure 1C,

$$\Delta V_T = s\ V_{T(b)} - s\ V_{ND} \quad (6)$$

where V_{ND} is the abscissa intercept. It is evident from the derivations that the Saturation and Occupancy plots have mutually inverted axes.

Source of Published Data

To use any one of the three linearizations, at least two consecutive PET recordings with two different levels of receptor occupancy are required. For the Inhibition plot, unlike the Saturation and Occupancy plots, the dependent ($V_{T(i)}$) and independent ($V_{T(b)}$) variables are not commingled. The estimates of the fractional receptor availability ($1 - s$) and V_{ND} are then obtained directly from the volumes of distribution. As the three linearizations are derived from the same original relative receptor availability formulation (Eq. 1), they must all meet the requirements that there are different brain regions with different receptor densities (maximum binding) that remain unchanged in the challenge condition and that the values of receptor affinity (Michaelis half-saturation concentration) and V_{ND} are the same for all relevant regions and remain the same for all challenges.

To assess the advantages and disadvantages of each of the three linearizations, the following names were searched in the PubMed and Scopus databases: "Lassen plot," "Saturation plot," "Gjedde plot," "Inhibition plot," "Cunningham plot," and "Occupancy plot." In the initial search, 60 published reports were found. The original datasets were not available for 36 of the identified studies.

Linear Regressions of Published Data

We analyzed the 24 remaining published reports, which consisted of 104 sets of data. In 7 cases, the authors submitted data (*8*,*17*–*22*), and for the remaining 17 reports, we extracted the data from published graphs with GetData Graph Digitizer digitization software (*11*,*13*,*23*–*37*). The characterization of the data in terms of species, sex, age, drug, dose, and other identifiers is presented in Table 1. We used two linear regression methods, LSM and DM, to obtain parameter estimates, as implemented in MATLAB (MathWorks). Using slope and intercept estimates, we determined s and V_{ND} and evaluated the accuracy.

LSM is a standard approach in regression analysis, with its most important application being in data fitting. The best fit of LSM minimizes the sum of squared residuals, which are the differences between an observed value and the value fitted by the model. In LSM, 2 variables (x,y) are obtained by regression of y on x, where x is assumed to represent independent-variable values obtained without error (*38*). DM regression is an errors-in-variables model that yields the line of best fit for a 2-dimensional dataset. It differs from LSM by the assumption of errors in both independent and dependent variables that allow for any number of predictors and a more complicated error structure. In DM, observations are subject to additive random variations of both x and y (*39*,*40*).

To test the goodness of fit of the linear regressions, we calculated the coefficient of determination (R^2), coefficient of variation (root-mean-square error [RMSE]), and infinity norm ($\|X\|_\infty$). The R^2 estimate is a commonly used indicator of the goodness of fit that is applicable only to LSM, as in other applications it may result in negative values or values greater than unity. In contrast, RMSE is applicable to all linear regressions. For n sets of (x_i; y_i) data, the RMSE, R^2, and $\|X\|_\infty$ measures can be expressed according to Rawlings et al. (*38*):

$$R^2 = 1 - \frac{SS_{res}}{SS_{tot}} \quad (7)$$

$$RMSE = \sqrt{SS_{res}/_n} \quad (8)$$

where n is the number of observations, and

$$\|X\|_\infty = \max(f_i - y_i) \quad (9)$$

where f_i is the predicted value of y at x_i, SS_{tot} is the total sum of squares or the variance of the data,

$$SS_{tot} = \sum_{i=1}^{n} (y_i - \bar{y})^2 \quad (10)$$

SS_{res} is sum of squares of residuals,

$$SS_{res} = \sum_{i=1}^{n} (f_i - y_i)^2 \quad (11)$$

and $\bar{y}$ is the mean of y_i,

$$\bar{y} = \frac{1}{n}\sum_{i=1}^{n} y_i \quad (12)$$

The closer the value of R^2 is to unity, the better the fit is to the linearization. The closer the RMSE and $\|X\|_\infty$ values are to zero, the better the fit of the linearization is held to be (*38*,*41*).

Calculation and Evaluation of Binding Potentials

We compared binding potential estimates (BP_{ND}) for the baseline (base BP_{ND}) and inhibition (challenge BP_{ND}) conditions according to Equation 3. In total, we compared 104 times 12, or 1,248, sets of BP_{ND} estimates according, first, to the equation for the percentage differences in the LSM and DM results for each of the 3 linearizations, exemplified here for the inhibition plot as

$$\Delta D_{(inhib)} = 100\frac{BP_{(LSM)} - BP_{(DM)}}{(BP_{(LSM)} + BP_{(DM)})/2} \quad (13)$$

and, second, according to the equation for the percentage differences in the three linearizations of each of the two regression methods, exemplified here for the comparison of LSM and DM results for the Inhibition and Occupancy plots,

$$\Delta D_{(LSM)} = 100\frac{BP_{(inhib)} - BP_{(occup)}}{(BP_{(inhib)} + BP_{(occup)})/2} \quad (14)$$

and

$$\Delta D_{(DM)} = 100\frac{BP_{(inhib)} - BP_{(occup)}}{(BP_{(inhib)} + BP_{(occup)})/2} \quad (15)$$

TABLE 1
Categorization of Data

Source	Cite	Case no.	Data no.	Type	Male	Female	Age (y)	Weight (kg)	Drug or material	Doses	Duration	Tracer
Owen et al. (*23*)	92	10	7–15	Human	—	—	—	—	XBD173	10–90 mg	—	^{11}C-PBR28
Naganawa et al. (*24*)	35	2	13	Human	—	—	25–52	—	PF-04455242	30 mg	1.5, 8 h	^{11}C-GR103545
Cunningham et al. (*13*)	197	4	9	Human	—	—	—	—	5HT 1A	1.5, 10, 150 μg/kg	1 h	^{11}C-WAY100635
Kågedal et al. (*25*)	31	3	10	Human	—	—	—	—	AZD2066	3.5, 6.9, 13.5 mg	—	^{11}C-ABP688
Jucaite et al. (*26*)	28	2	9	Human	2	0	22–44	—	AZD5213	0.1, 0.3 mg	2 h	^{11}C -GSK189254, ^{11}C-AZ12807110
Elmenhorst et al. (*27*)	57	14	9–23	Human	—	—	24–68	—	Caffeine	0–9 mg/kg	36 h	^{18}F-CP FPX
Ridler et al. (*28*)	24	6	12–15	*Papio anubis*	6	0	—	22.4	P943, SB-616234-S, SB-714786	25, 100 μg	—	^{11}C-P943
Fuchigami et al. (*29*)	3	2	6	Rhesus monkey	—	—	—	4.90, 5.55	SSR504734	1.5 and 4.5 mg/kg	—	^{11}C-*N*-methyl-SSR504734
Logan et al. (*30*)	4	1	7	Human	—	—	23–67	—	Letrozole	2.5 mg	2.5 h	^{11}C-Vorozol e
Martin-Facklam et al. (*31*)	38	5	26–39	Human	5	—	20–51	—	Bitopertin	5, 15, 30, 60, 175 mg	—	^{11}C-RO5013853
Lassen et al. (*11*)	18	1	31	Human	1	0	22–65	—	Benzodiazepines	0.6 mg	—	^{11}C-flumazenil
Myers et al. (*32*)	19	12	24	Human	—	—	Avg: 43,44	—	Zolpidem, placebo	1.37–3.71 μg	1.5 h	^{11}C-flumazenil, ^{11}C-Ro15-4513
Phan et al. (*33*)	1	1	9	Sprague–Dawley rats	0	1	—	0.225–0.250	Cyclosporine	1 mg/kg	1.5 h	^{11}C-yohimbine
Ettrup et al. (*19*)	41	5	10	Danish Landrace pigs	0	5	—	19	SSR180711 NS14492	1, 10 mg/kg	0.5, 4 h	^{11}C-NS14492
Ramakrishnan et al. (*18*)	4	2	12	Wistar Hannover rat	2	0	—	—	Cutamesine	0.3, 1 mg/kg	—	^{11}C-SA4503
Visser et al. (*34*)	5	1	11	Wistar rats	1	0	—	0.317	MDL 100907	1 mg/mL	—	^{11}C-MDL 100907
Milak et al. (*35*)	53	6	8	*Papio anubis*	6	0	—	—	Citalopram, fenfluramine	2, 2.5, 4 mg/kg	—	^{11}C-CUMI-101
Hillmer et al. (*36*)	12	3	9	*Macaca mulatta*	2	1	6–15	7–14	ASEM	0.69, 1.24 mg/kg	—	^{18}F-DBT-10
Paul et al. (*37*)	11	2	14	Wistar rats	2	0	—	0.304	CPA, caffeine	0.25, 40 mg/kg	15 min	^{11}C-MPDX
Phan et al. (*8*)	11	10	6	Sprague–Dawley rats	—	—	—	0.250–0.300	Amphetamine	—	6–28 min	^{11}C-yohimbine
Horti et al. (*17*)	41	2	16	Baboon	2	0	—	20.1–26.0	ASEM	0.5, 5 mg/kg	5–90 min	^{18}F-ASEM
Narendran et al. (*20*)	28	6	11	Human	5	1	Avg: 24	—	Aripiprazole	15 mg	3	^{11}CFLB 457
Koole et al. (*22*)	12	3	15	Human	—	—	20–54		Padsevonil	6.25 mg	2	^{11}C-UCB-J
Wong et al. (*21*)	12	1	20	Human	1	0	18–52	—	DMXB-A	150 mg	40 min	^{18}F-ASEM

Avg = average.

Goodness of Fit

We considered sets of data ($V_{T(b)}$, $V_{T(i)}$) directly measured in relevant studies. Because of sources of error, which include surgery, environment, and device errors, we predicted differences to exist between the theoretic but unknown value of a parameter and the measured value (*42*). We expressed the theoretic value of a parameter as ($V_{T(b)}$, $V_{T(i)}$),

$$V^*_{T(i)} = V_{T(i)} - e_1 \quad (16)$$

and

$$V^*_{T(b)} = V_{T(b)} - e_2 \quad (17)$$

where e_1 and e_2 are the differences between real and measured values of $V_{T(b)}$ and $V_{T(i)}$, respectively. We expressed the real value of the differences between baseline and inhibition volumes of distribution as ΔV^*_T,

$$\Delta V^*_T = V^*_{T(i)} - V^*_{T(b)},$$

which after substitution yielded,

$$\Delta V^*_T = \left(V_{T(i)} - e_1\right) - \left(V_{T(b)} - e_2\right)$$

or

$$\Delta V^*_T = \left(V_{T(i)} - V_{T(b)}\right) - (e_1 - e_2),$$

which yielded,

$$\Delta V^*_T = \left(V_{T(i)} - V_{T(b)}\right) - (e_3) \quad (18)$$

where e_3 refers to the difference between the real and measured values of ΔV_T.

Source of Convergence

In this research, we defined the closeness of the fitted model to the data as convergence. For the set of (x_i; y_i), regardless of method, the linearization has the form,

$$y = ax + b \quad (19)$$

with the real values in the equation expressed as,

$$y = a^*x + b^* \quad (20)$$

where (a,b) are the estimated values of slope and ordinate intercept and (a^*,b^*) are the real values of slope and ordinate intercept. As discussed, the measurement error of (x_i; y_i) yields a difference between real and estimated values of slope and ordinate intercept as

$$a^* = a - e^*_1 \quad (21)$$

and

$$b^* = b - e^*_2 \quad (22)$$

where e^*_1 is the error between real and estimated values of slope and ordinate intercept. By substituting Equations 20 and 21 in the 3 original equations (Eqs. 4–6), we calculated the differences between real and estimated values of s and V_{ND}. Here, occupancy and V_{ND} are the estimated values, and s* and V_{ND}* are the real (unknown) values. The differences between the real and estimated values of s and V_{ND} are listed in Table 2.

TABLE 2
Differences Between Real and Estimated Values of s and V_{ND} of Inhibition, Occupancy, and Saturation Plots

Method	*s*	V_{ND}
Inhibition	$s^* + e_1$	$\frac{s^*V^*_{ND} - e_1}{s^* + e_1}$
Occupancy	$s^* - e_1$	$\frac{s^*V^*_{ND} - e_1}{s^* - e_1}$
Saturation	$\frac{s^*}{1 - s^* - e_1}$	$V^*_{ND} - e_2$

RESULTS

Digitization Accuracy

We compared the linearizations of data obtained from the authors directly or by digitization of published graphs. With the submitted data available for comparison, we showed the mean error of digitization to be less than 0.85%, confirming the accuracy of the digitization. Here, we present the results from the analysis of the digitized values of $V_{T(b)}$ and ΔV_T from the report of Horti et al. (*17*), used to obtain the $V_{T(i)}$ values for the 0.5-mg receptor inhibitor challenge. With the Inhibition, Saturation, and Occupancy linearizations for the LSM and DM regressions, we obtained the parameter values from the linear regressions of the data presented in Figure 1, with the resulting regressions and estimates of s and V_{ND} being presented in Figure 2. For the Saturation plot, we used ΔV_T as the independent variable (x) and $V_{T(b)}$ as the dependent variable (y), whereas for the Occupancy plot, we used

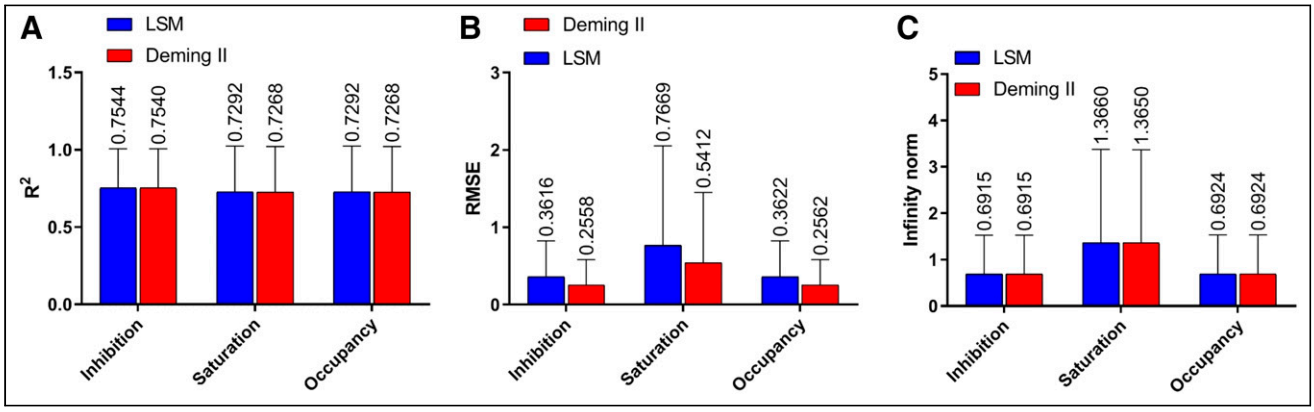

FIGURE 2. Average values of measures of goodness of fit of the Inhibition, Saturation, and Occupancy plots.

TABLE 3
Average Precision of Regressions of Inhibition, Occupancy, and Saturation Plots

Plot	Method	R^2	RMSE	$\|X\|_\infty$
Inhibition	LSM	0.75 ± 0.25	0.36 ± 0.46	0.69 ± 0.84
	DM	0.75 ± 0.25	0.26 ± 0.33	0.69 ± 0.84
Saturation	LSM	0.73 ± 0.29	0.77 ± 1.29	1.40 ± 2.01
	DM	0.73 ± 0.29	0.55 ± 0.91	1.40 ± 2.01
Occupancy	LSM	0.73 ± 0.29	0.36 ± 0.46	0.69 ± 0.84
	DM	0.73 ± 0.29	0.26 ± 0.33	0.69 ± 0.84

ΔV_T as the dependent variable (y) and $V_{T(b)}$ as the independent variable (x).

Plot Analysis

Using the linearization goodness-of-fit parameters R^2, RMSE, and $\|X\|_\infty$, the comparisons yielded the results listed in Table 3 and Figure 2. The mean value of R^2 (for the 104 samples) for the Inhibition plot was slightly closer to unity, identifying the Inhibition plot as the plot with slightly greater fit to the experimental data. In addition, the mean values of RMSE and $\|X\|_\infty$ for the Inhibition plot were closest to zero, again as the most accurate of the three plots. In 87 of the 104 cases, the Inhibition plot yielded the lowest RMSE and $\|X\|_\infty$ values, implying that the inhibition plot had superior accuracy in the 87 cases.

The effects of the regression method (LSM or DM) on the estimated values of s, V_{ND}, and BP_{ND} are shown in Figure 3. The estimates of s, V_{ND}, and BP_{ND} for the two regression methods (LSM and DM) generally converged. The average deviation was less than 0.1% for s and V_{ND} and was less than 3% for BP_{ND}. We also compared the effects of choice of method on the estimated values of s, V_{ND}, and BP_{ND}. The deviations of s, V_{ND}, and BP_{ND} for the three plots (Inhibition, Saturation, and Occupancy) are shown in Figure 3. From the figure, we conclude that the results of the Inhibition and Occupancy plots normally converged for both LSM and DM. The average difference of the inhibition and occupancy plot results was less than 2%. In contrast, we generally found considerable differences between the results of the Saturation plot and the results of the Inhibition and Occupancy plots. The average difference shown in Figure 3 is close to 40%. Bland–Altman graphs for the binding potentials determined with 0.5-mg receptor inhibitor blockade by Horti et al. (*17*) are shown in Supplemental Figure 1 (supplemental materials are available at http://jnm.snmjournals.org).

Analysis of Noise Simulation

To investigate the effect of noise on the convergence of the results of different plots, two sets of theoretic data (data without noise) were created on the basis of the Horti et al. (*17*) data at two levels of inhibition (0.5- and 5-mg inhibitor administration). We considered five sets of data and calculated the values of s and of V_{ND} using the three plots and two different linearizations (data without noise; data with noise of K = 0.1, K = 0.2, K = 0.5, where K is the chosen SD). The results of the linearizations are listed in Supplemental Table 1 and Supplemental Figure 2. As shown in Supplemental Figure 3, for the data without noise, all

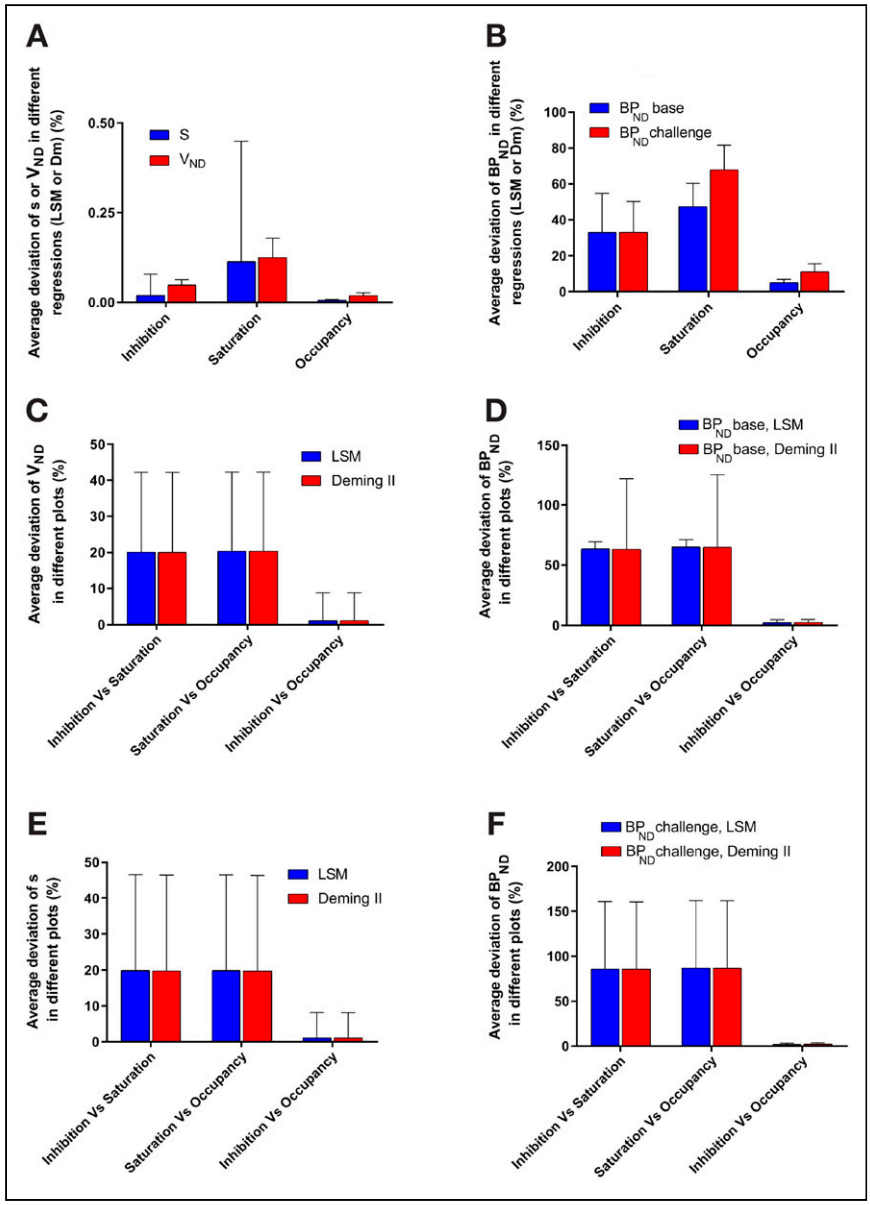

FIGURE 3. Differences of s, V_{ND}, and BP_{ND} among Inhibition, Saturation, and Occupancy plots. (A) s and V_{ND} LSM vs. Deming II. (B) BP_{ND} LSM vs. Deming II. (C) V_{ND} LSM and Deming II in different plots. (D) BP_{ND} Base LSM and Deming II in different plots. (E) s LSM and Deming II in different plots. (F) BP_{ND} Challenge LSM and Deming II in different plots.

three plots and two linearizations yield identical results. For the convergence of the three plots, it is evident that the RMSE of the data without noise for all three plots is approximately zero (10^{-9}). However, as is shown in Supplemental Figure 4, in the presence of noise, the inhibition and occupancy plots yielded a lower RMSE, consistent with greater convergence.

DISCUSSION

In the present examination of the plots of competition, we linearized the formulation of the fractional receptor availability (Eq. 1) into three equations underlying the different regressions, which we refer to as the Saturation, Inhibition, and Occupancy plots. The purpose of all three linearizations is to estimate the reference volume of distribution, V_{ND}, required to calculate the binding potential of a radioligand. We undertook the comparisons because the extent to which the results of the three plots converge or diverge is unknown. We culled 104 cases on the basis of one or more of the plots, and we tested the results of the three plots linearized by LSM and DM regressions.

As shown in Table 3, for both s and V_{ND}, the differences between estimated and real values are of the same order of magnitude for the Inhibition and Occupancy plots but are much greater for the Saturation plot. For this reason, the average deviation of the calculated values of s and V_{ND} for the Inhibition and Occupancy plots was less than 0.1%, and the results generally converged. In contrast, there was more than a 35% difference between the results of the Saturation plots and the results of the Inhibition and Occupancy plots. In Equations 16–18, e_1, e_2, and e_3 are the error values resulting from the divergence of individual plots. The parameter e_3 may be smaller than e_1 and e_2 but frequently is not. As e_1 and e_2 do not adopt exclusively positive or negative values, errors can be superimposed. For this reason, the use of ΔV_T differences may result in higher levels of error and reductions of goodness of fit. Among the three methods, the Inhibition plot avoided the use of the commingled variable ΔV_T. As expressed by the three indicators R^2, RMSE, and $\|X\|_\infty$, the Inhibition plot was shown to yield slightly greater fit for both LSM and DM. The noise analysis showed that the Inhibition and Occupancy plots yielded higher convergence in the presence of noise.

CONCLUSION

On the basis of all three goodness-of-fit parameters (R^2, RMSE, and $\|X\|_\infty$), and using both regression methods (LSM and DM), the Inhibition and Occupancy plots emerged as the plots with a superior degree of convergence. We judge this to be in part because of the absence of commingling of the original dependent and independent variables of the Saturation (original Lassen) plot. Concerning the effect of regression method (LSM and DM) on the estimated values of s, V_{ND}, and BP_{ND}, we observed that the average differences in the results of the Inhibition and Occupancy plot linearizations were less than 0.1% and, as such, negligible. In contrast, we noted more than a 35% difference in the results of the Saturation plot comparisons—a difference that we explain by the violation of the negligible variability rule for independent variables. The noise analysis showed that the three plots resulted in the same parameter estimates in the absence of noise. However, in the presence of noise, the Inhibition and Occupancy plots yielded higher and close degrees of convergence.

DISCLOSURE

This study was supported by Parkinsonforeningen, Lundbeckfonden (R77-A6970), and the Danish Agency for Science and Higher Education. No other potential conflict of interest relevant to this article was reported.

KEY POINTS

QUESTION: Which of the three linearizations (Inhibition, Saturation, and Occupancy) had superior convergence with the experimental results?

PERTINENT FINDINGS: Superior convergences among the values of s, V_{ND}, and BP_{ND} were observed for the Inhibition and Occupancy plots. On the basis of the goodness-of-fit parameters (R^2, RMSE, and $\|X\|_\infty$) and with both regression methods (LSM and DM), the Inhibition plot emerged as the plot with the slightly higher degree of convergence.

IMPLICATIONS FOR PATIENT CARE: The correct use of the Occupancy and Inhibition plots allows brain-imaging specialists to advise on the optimal dose of target engagement of neuroreceptor inhibitor drugs chosen to block the pathologic excess of neurotransmission.

REFERENCES

1. Ter-Pogossian MM. Positron emission tomography. In: *Biomedical Images and Computers*. Springer; 1982:216–224.
2. Gjedde A, Wong DF, Rosa-Neto P, Cumming P. Mapping neuroreceptors at work: on the definition and interpretation of binding potentials after 20 years of progress. *Int Rev Neurobiol.* 2005;63:1–20.
3. Wahl RL. Current status of PET in breast cancer imaging, staging, and therapy. *Semin Roentgenol.* 2001;36:250–260.
4. Wong DF, Gjedde A, Wagner HN Jr. Quantification of neuroreceptors in the living human brain. I. Irreversible binding of ligands. *J Cereb Blood Flow Metab.* 1986; 6:137–146.
5. Phan J-A, Landau AM, Jakobsen S, Wong DF, Gjedde A. Radioligand binding analysis of α 2 adrenoceptors with [^{11}C] yohimbine in brain in vivo: extended inhibition plot correction for plasma protein binding. *Sci Rep.* 2017;7:15979.
6. Naganawa M, Gallezot J-D, Rossano S, Carson RE. Quantitative PET imaging in drug development: estimation of target occupancy. *Bull Math Biol.* 2019;81: 3508–3541.
7. Gjedde A, Wong DF, Wagner Jr HN. Transient analysis of irreversible and reversible tracer binding in human brain in vivo. In: *PET and NMR: New Perspectives in Neuroimaging and in Clinical Neurochemistry.* AR Liss; 1986:223–235.
8. Phan J-A, Landau AM, Wong DF, et al. Quantification of [^{11}C] yohimbine binding to α2 adrenoceptors in rat brain in vivo. *J Cereb Blood Flow Metab.* 2015;35: 501–511.
9. Landau AM, Alstrup AK, Audrain H, et al. Elevated dopamine D1 receptor availability in striatum of Göttingen minipigs after electroconvulsive therapy. *J Cereb Blood Flow Metab.* 2018;38:881–887.
10. DeLorenzo C, Gallezot J-D, Gardus J, et al. In vivo variation in same-day estimates of metabotropic glutamate receptor subtype 5 binding using [^{11}C] ABP688 and [^{18}F] FPEB. *J Cereb Blood Flow Metab.* 2017;37:2716–2727.
11. Lassen NA, Bartenstein P, Lammertsma A, et al. Benzodiazepine receptor quantification in vivo in humans using [^{11}C] flumazenil and PET: application of the steady-state principle. *J Cereb Blood Flow Metab.* 1995;15:152–165.
12. Gjedde A, Wong D. Receptor occupancy in absence of reference region [abstract]. *Neuroimage.* 2000;11(suppl):S48.
13. Cunningham VJ, Rabiner EA, Slifstein M, Laruelle M, Gunn RN. Measuring drug occupancy in the absence of a reference region: the Lassen plot re-visited. *J Cereb Blood Flow Metab.* 2010;30:46–50.
14. Mintun MA, Raichle ME, Kilbourn MR, Wooten GF, Welch MJ. A quantitative model for the in vivo assessment of drug binding sites with positron emission tomography. *Ann Neurol.* 1984;15:217–227.
15. Karalija N, Jonassson L, Johansson J, et al. High long-term test–retest reliability for extrastriatal ^{11}C-raclopride binding in healthy older adults. *J Cereb Blood Flow Metab.* 2020;40:1859–1868.

16. Innis RB, Cunningham VJ, Delforge J, et al. Consensus nomenclature for in vivo imaging of reversibly binding radioligands. *J Cereb Blood Flow Metab.* 2007;27: 1533–1539.
17. Horti AG, Gao Y, Kuwabara H, et al. ^{18}F-ASEM, a radiolabeled antagonist for imaging the α7-nicotinic acetylcholine receptor with PET. *J Nucl Med.* 2014;55: 672–677.
18. Ramakrishnan NK, Schepers M, Luurtsema G, et al. Cutamesine overcomes REM sleep deprivation-induced memory loss: relationship to sigma-1 receptor occupancy. *Mol Imaging Biol.* 2015;17:364–372.
19. Ettrup A, Mikkelsen JD, Lehel S, et al. ^{11}C-NS14492 as a novel PET radioligand for imaging cerebral α7 nicotinic acetylcholine receptors: in vivo evaluation and drug occupancy measurements. *J Nucl Med.* 2011;52:1449–1456.
20. Narendran R, Mason NS, Chen CM, et al. Evaluation of dopamine $D_{2/3}$ specific binding in the cerebellum for the positron emission tomography radiotracer [^{11}C] FLB 457: implications for measuring cortical dopamine release. *Synapse.* 2011;65: 991–997.
21. Wong DF, Kuwabara H, Horti AG, et al. Brain PET imaging of α7-nAChR with [^{18}F] ASEM: reproducibility, occupancy, receptor density, and changes in schizophrenia. *Int J Neuropsychopharmacol.* 2018;21:656–667.
22. Koole M, van Aalst J, Devrome M, et al. Quantifying SV2A density and drug occupancy in the human brain using [^{11}C] UCB-J PET imaging and subcortical white matter as reference tissue. *Eur J Nucl Med Mol Imaging.* 2019;46:396–406.
23. Owen DR, Guo Q, Kalk NJ, et al. Determination of [^{11}C] PBR28 binding potential in vivo: a first human TSPO blocking study. *J Cereb Blood Flow Metab.* 2014;34: 989–994.
24. Naganawa M, Jacobsen LK, Zheng M-Q, et al. Evaluation of the agonist PET radioligand [^{11}C] GR103545 to image kappa opioid receptor in humans: kinetic model selection, test–retest reproducibility and receptor occupancy by the antagonist PF-04455242. *Neuroimage.* 2014;99:69–79.
25. Kågedal M, Cselényi Z, Nyberg S, et al. A positron emission tomography study in healthy volunteers to estimate mGluR5 receptor occupancy of AZD2066: estimating occupancy in the absence of a reference region. *Neuroimage.* 2013;82: 160–169.
26. Jucaite A, Takano A, Boström E, et al. AZD5213: a novel histamine H3 receptor antagonist permitting high daytime and low nocturnal H3 receptor occupancy, a PET study in human subjects. *Int J Neuropsychopharmacol.* 2013;16:1231–1239.
27. Elmenhorst D, Meyer PT, Matusch A, Winz OH, Bauer A. Caffeine occupancy of human cerebral A1 adenosine receptors: in vivo quantification with ^{18}F-CPFPX and PET. *J Nucl Med.* 2012;53:1723–1729.
28. Ridler K, Plisson C, Rabiner EA, et al. Characterization of in vivo pharmacological properties and sensitivity to endogenous serotonin of [^{11}C] P943: a positron emission tomography study in *Papio anubis. Synapse.* 2011;65:1119–1127.
29. Fuchigami T, Takano A, Gulyás B, et al. Synthesis and evaluation of 2-chloro *N*-[(*S*)-{(*S*)-1-[^{11}C] methylpiperidin-2-yl}(phenyl) methyl] 3-trifluoromethyl-benzamide ([^{11}C] *N*-methyl-SSR504734) as a PET radioligand for glycine transporter 1. *EJNMMI Res.* 2012;2:37.
30. Logan J, Kim SW, Pareto D, et al. Kinetic analysis of [^{11}C] vorozole binding in the human brain with positron emission tomography. *Mol Imaging.* 2014;13:1–12.
31. Martin-Facklam M, Pizzagalli F, Zhou Y, et al. Glycine transporter type 1 occupancy by bitopertin: a positron emission tomography study in healthy volunteers. *Neuropsychopharmacology.* 2013;38:504–512.
32. Myers JF, Rosso L, Watson BJ, et al. Characterisation of the contribution of the GABA-benzodiazepine α1 receptor subtype to [^{11}C] Ro15-4513 PET images. *J Cereb Blood Flow Metab.* 2012;32:731–744.
33. Phan J-A, Jakobsen S, Landau AM, Doudet D, Gjedde A. Amphetamine-induced inhibition of [C-11] yohimbine binding in rat brain. *J Cereb Blood Flow Metab.* 2012;32(suppl):S98–S99.
34. Visser AK, De Vries EF, Ramakrishnan NK, et al. Analysis of 5-HT 2A receptor binding with [^{11}C] MDL 100907 in rats: optimization of kinetic modeling. *Mol Imaging Biol.* 2013;15:730–738.
35. Milak MS, Severance AJ, Prabhakaran J, et al. In vivo serotonin-sensitive binding of [^{11}C] CUMI-101: a serotonin 1A receptor agonist positron emission tomography radiotracer. *J Cereb Blood Flow Metab.* 2011;31:243–249.
36. Hillmer AT, Zheng M-Q, Li S, et al. PET imaging evaluation of [^{18}F] DBT-10, a novel radioligand specific to α 7 nicotinic acetylcholine receptors, in nonhuman primates. *Eur J Nucl Med Mol Imaging.* 2016;43:537–547.
37. Paul S, Khanapur S, Sijbesma JW, et al. Use of ^{11}C-MPDX and PET to study adenosine A1 receptor occupancy by nonradioactive agonists and antagonists. *J Nucl Med.* 2014;55:315–320.
38. Rawlings JO, Pantula SG, Dickey DA. *Applied Regression Analysis: A Research Tool.* Springer Science and Business Media; 2001:2–6.
39. Deming WE. *Statistical Adjustment of Data.* Dover Publications; 1943:59–127.
40. Linnet K. Estimation of the linear relationship between the measurements of two methods with proportional errors. *Stat Med.* 1990;9:1463–1473.
41. Epperson JF. *An Introduction to Numerical Methods and Analysis.* John Wiley and Sons; 2013:442–444.
42. Sydenham PH, Thorn R. *Handbook of Measuring System Design.* John Wiley and Sons; 2005:289–300.